



No reference quality evaluation for screen content images considering texture feature based on sparse representation

Jiachen Yang^a, Jiacheng Liu^{a,*}, Bin Jiang^a, Wen Lu^b

^a School of Electrical and Information Engineering, Tianjin University, Tianjin 30072, China

^b School of Electronic Engineering, Xidian University, Xian, Shaanxi 710071, China

ARTICLE INFO

Article history:

Received 30 May 2018

Revised 8 July 2018

Accepted 10 July 2018

Available online 1 August 2018

Keywords:

Screen content images

Sparse representation

No reference

Texture information

ABSTRACT

In this paper, an accurate blind metric evaluating screen content images (SCIs) considering texture feature via sparse representation is proposed. The existing theory on human vision tells us that human visual system (HVS) is sensitive to texture information of images. In addition, gradient direction has not been adequately explored as a predictive information source of SCIs. This method is first based on three kinds of gradient maps of SCIs—i.e., *gradient magnitude map*, *relative gradient direction map*, *relative gradient magnitude map*. Since the existing literatures about human neuroscience have revealed that image texture can be captured by high-order derivatives, texture information of SCIs can be represented by local histogram of oriented gradient (HOG) features extracted from the aforementioned gradient maps. Finally, it is composed of two important procedures: representing HOG features by means of sparse coding, then weighting subjective experimental quality scores via the sparse coding coefficients to predict objective perceptive quality scores of SCIs. Comparison experiments on the public SCI database demonstrate that the designed metric has the better superiority over existing the-state-of-art algorithms and delivers consistency and accuracy in relation with subjective evaluation.

© 2018 Elsevier B.V. All rights reserved.

1. Introduction

With the rapid development of the network and numerous electronic digital devices, images that people contact with in daily life are not only natural images, but also screen content images (SCIs). Natural images are captured by cameras, while screen content images are captured by computers or other electronic digital devices. As can be seen from Fig. 1(a) and (b), the difference between the SCI and the natural image is quite obvious. Natural images contain fewer lines and more uniform color information distribution, whereas SCIs are the opposite. In terms of statistical Mean Subtracted Contrast Normalized (MSCN) coefficients, as shown in Fig. 1(c) and (d), the MSCN coefficients of the natural image can fit well with the NSS model, which displays a Gaussian-like form, while the SCI demonstrates a Laplacian-like MSCN distribution with great differences. For their four types of common distorted versions (e.g., Gaussian blur, Gaussian noise, JPEG compression and JPEG2K compression), the distributions of MSCN coefficients of natural images are symmetrical while those of SCIs are asymmetrical in the figure. In the process of image acquisi-

tion, transmission and coding, the visual perception of SCIs will be degraded because of the introduction of various distortions. For example, teleconferencing and online cloud videos are affected by transmission distortions, network delays and other adverse factors, all of which require online real-time SCI quality evaluating, so as to facilitate the service providers to dynamically adjust the source location strategy to meet the demands of service quality. Thus, it is essential to raise an effective quality assessment method for SCIs.

The local direction of gradient images contains significant information regarding object structure of image [1]. The visual quality of SCIs is correlated with the gradient direction, which can be changed by distortion types of SCIs. Therefore, a feasible way to solve the visual quality assessment issue for SCIs is to analyze the structural information of gradient direction. In this paper, a novel blind framework is put forward based on sparse representation to assess the perceptive quality of SCIs. It is supposed that there is an underlying relationship between the texture feature vector and the subjective quality vector. The method we put forward is unique in the following aspects:

(1) As one of the most important characteristics of the human visual system (HVS), sparsity in human visual perception has been strongly reinforced by neuroscience. Sparse representation is adopted in the proposed scheme and produces the better prediction accuracy for SCIs in experiment.

* Corresponding author.

E-mail addresses: yangjiachen@tju.edu.cn (J. Yang), liujc9508@tju.edu.cn (J. Liu), jiangbin@tju.edu.cn (B. Jiang), luwen@mail.xidian.edu.cn (W. Lu).

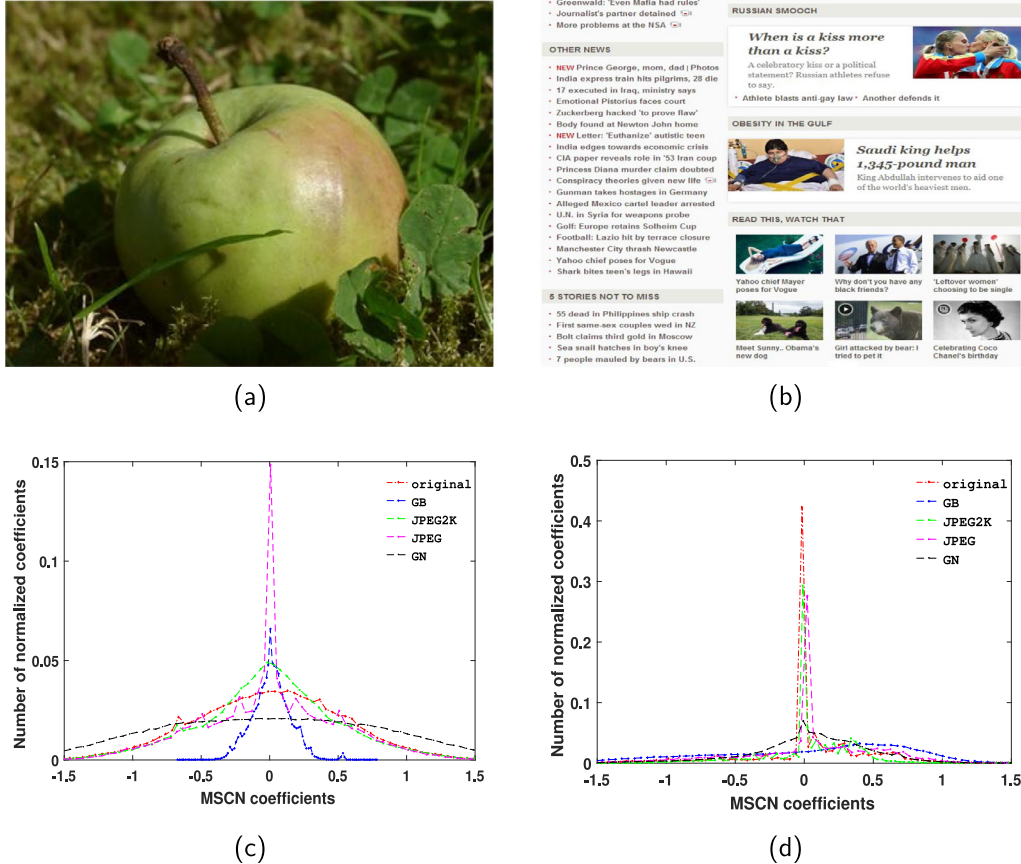


Fig. 1. The difference between natural images and SCIs. (a) and (b) original natural image and SCI; (c) and (d) histograms of MSCN coefficients of original and distortion types of (a) and (b) corrupted by Gaussian blur, Gaussian noise, JPEG compression and JPEG2K compression.

(2) The potential of the gradient direction in SCIs is further explored in this paper. Therefore, a new blind scheme considering the relative gradient direction is designed for perceptive quality evaluation of SCIs.

(3) Human visual perception is sensitive to the area of high contrast, such as texture and edge. Thus, we extract HOG features as second-order derivatives from first-order gradient information, which represents the texture information well.

The rest of this paper is described as follows. Section 2 briefly reviews the related work. Section 3 demonstrates the designed visual quality evaluation metric for SCIs in detail. Experimental results conducted on the screen content image database are provided, so as to verify the effectiveness of our designed scheme against several representative quality schemes, as presented in Section 4. The conclusion is drawn in Section 5.

2. Related work

In the past few years, there have been a number of sophisticated objective models for assessing the perceptive quality of natural images (IQA) and many relevant algorithms have been proposed [2,3]. Numerous advanced full reference (FR) algorithms were designed, such as the peak signal-to-noise ratio (PSNR), the structural similarity index (SSIM) [4], the multiscale structural similarity index (MS-SSIM) [5], feature similarity (FSIM) [6], visual information fidelity (VIF) [7], internal generative mechanism (IGM) [8], visual saliency-induced index (VSI) [9] and so on. There have been also some IQA methods designed considering one kind of local structure descriptor: the histograms of oriented gradients (HOG). Wang et al. [10] presented the M-HOG model by calculating the distance of HOG descriptor. Yang et al. [11] developed a HOG-M

model via combining HOG descriptor with the SSIM method. Differing from FR schemes, NR schemes are more desirable to assess the image visual quality without information of the original image. In the existing paper, there are several classical no reference (NR) quality evaluation models, such as distortion identification based image verity and integrity evaluation (DIIVINE) [12], blind/referenceless image spatial quality evaluator (BRISQUE) [13], natural image quality evaluator (NIQE) [14], the integrated-local NIQE (IL-NIQE) [15], blind image integrity notator using DCT statistics (BLIINDS-II) [16], the quality-aware clustering (QAC) [17], edge-feature-based image segmentation (EFS) [18], matching-pursuit-based algorithm [19] and so on. There are also deep learning based NR metrics [20,21]. All these schemes are presented in a similar way, which extracts some features representing image visual quality and then applies the extracted features to train the predictive model. Besides FR and NR models, a great deal of reduced-reference (RR) quality evaluating algorithms have been designed lately, which essentially make quality decisions considering partial features as the indicators of general image features [22–26].

In the existing literature about IQA metrics, most of them are designed to evaluate the visual quality for natural images. Apparently, IQA metrics are not ideal for predicting the visual quality of SCIs because the structural information and statistical characteristics of SCIs have great differences with natural images, such as the aforementioned MSCN coefficients. The significant difference from natural images is that SCI consists of many varieties of visual perceptual regions, such as pictorial and textual areas [27]. Recently, there are several quality assessment models for SCIs. Yang et al. [28] proposed a FR IQA scheme for SCIs to evaluate the perceptive quality of pictorial and textual areas separately. Gu et al. [29] pre-

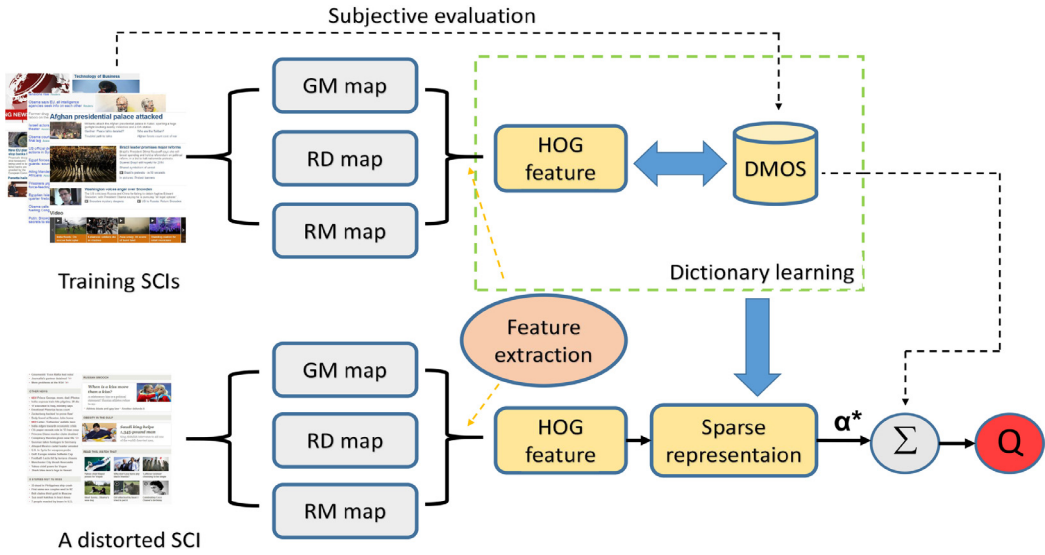


Fig. 2. Flowchart of the proposed scheme.

sented a FR IQA model for SCIs by weighting SSIM measurement with structural degradation means. Wang et al. [30] put forward a FR IQA model for SCIs by combining local information content weighting with the adaptability of view fields. Gu et al. [31] proposed a FR IQA scheme for SCIs via exploiting the saliency-guided gradient magnitude similarity. Wang et al. [32] put forward a RR IQA algorithm for SCIs considering primary visual information and uncertainty quantity. Zuo et al. [33] designed a NR IQA model for SCIs to predict the visual quality of pictorial part and textual part in SCIs via a CNN network separately. Ni et al. [34] put forward a FR IQA model for SCIs (ESIM) using a parametric edge model and gradient direction. Fang et al. [35] presented a FR IQA scheme for SCIs considering uncertainty weighting. Wang et al. [36] designed a RR IQA model for SCIs in wavelet domain. Shao et al. [37] developed a NR quality predictor for SCIs (BLIQUP-SCI) via global and local sparse representation. Gu et al. [38] presented a blind metric for SCIs using four kinds of features to build an IQA skeleton based on big data learning. Lu and Li [39] proposed a blind metric for SCIs by orientation selectivity mechanism. Fang et al. [27] developed a NRTL scheme for SCIs by using global luminance and local texture information. Although these NR IQA metrics designed for SCIs have solved the problem of assessing the quality of SCIs, they do not yield visual quality estimates that are consistent with human perception enough. Designing superior NR IQA metrics for SCIs is still challenging in the following study.

In the research field of traditional image quality assessment, there is a transition process from the gradient magnitude to the gradient direction. General approaches in existing literatures (e.g., [1,6,40,41]) use the gradient magnitude to obtain certain features characterizing the image, while the gradient direction was not taken into account enough. Although Liu et al. [42] used the gradient direction in their proposed models, their proposed metrics evaluated the visual quality for natural images, which failed to maintain the reasonable predictive accuracy for SCIs. With the extensive application of SCIs, there have been several methods (e.g., [32,34,35,43]) based on the gradient magnitude or direction for SCIs in recent years. Nevertheless, they all belong to the FR or RR methods.

3. The proposed framework

As we can see, the SCI consists of the pictorial region and textual region. Since HVS is sensitive to edge information, which is

the basic component in regions full of texts and high-frequency parts of the pictorial regions in SCIs [27], the gradient feature of SCI is related to its visual quality. Therefore, a blind quality evaluation scheme for SCIs is designed via sparse representation as demonstrated in Fig. 2. Firstly, a dictionary is built by combining a set of SCIs with different distorted versions. Next HOG features extracted from gradient maps are encoded in the dictionary by means of sparse representation. Finally, the coding coefficients are exploited to linearly weight the corresponding differential mean opinion score (DMOS) to predict the objective scores of SCIs. Each procedure will be demonstrated in the following subsections in detail.

3.1. Gradient magnitude and gradient direction in SCIs

The gradient magnitude (GM) of SCIs will be modified when they are corrupted by various distorted types. For example, the introduction of Gaussian blur or motion blur will reduce the gradient magnitude values of SCIs, and the compression distortion in SCIs, such as JPEG, JPEG2K and LSC, will change the location of the gradient magnitude in the original SCI. But the changes are not obvious in the histogram of the gradient magnitude distributions. For the gradient direction (GD), not only the distribution of spatial gradient location is modified, but also the difference between the original SCI and its distorted version is clearly separated in the histogram of gradient direction distribution. It can be concluded that the gradient direction of SCIs suffering from various kinds of distortions will modify the image anisotropies. In order to validate our theory, we make a comparison between an original SCI and its JPEG distorted type in Figs. 3 and 4.

3.2. Computation of three types of gradient maps

As introduced above, the gradient magnitude (GM) of a SCI is at the pixel point (x, y) expressed as

$$F(x, y) = |F_h(x, y)| + |F_v(x, y)| \quad (1)$$

where the symbol $| \cdot |$ represents the absolute value of the pointed quantity. In the process of calculating the gradient, l_1 norm is applied instead of l_2 norm since the overall amount of gradient variations (regardless of the horizontal direction or vertical direction) is an effective stimulus to the human eye perception and

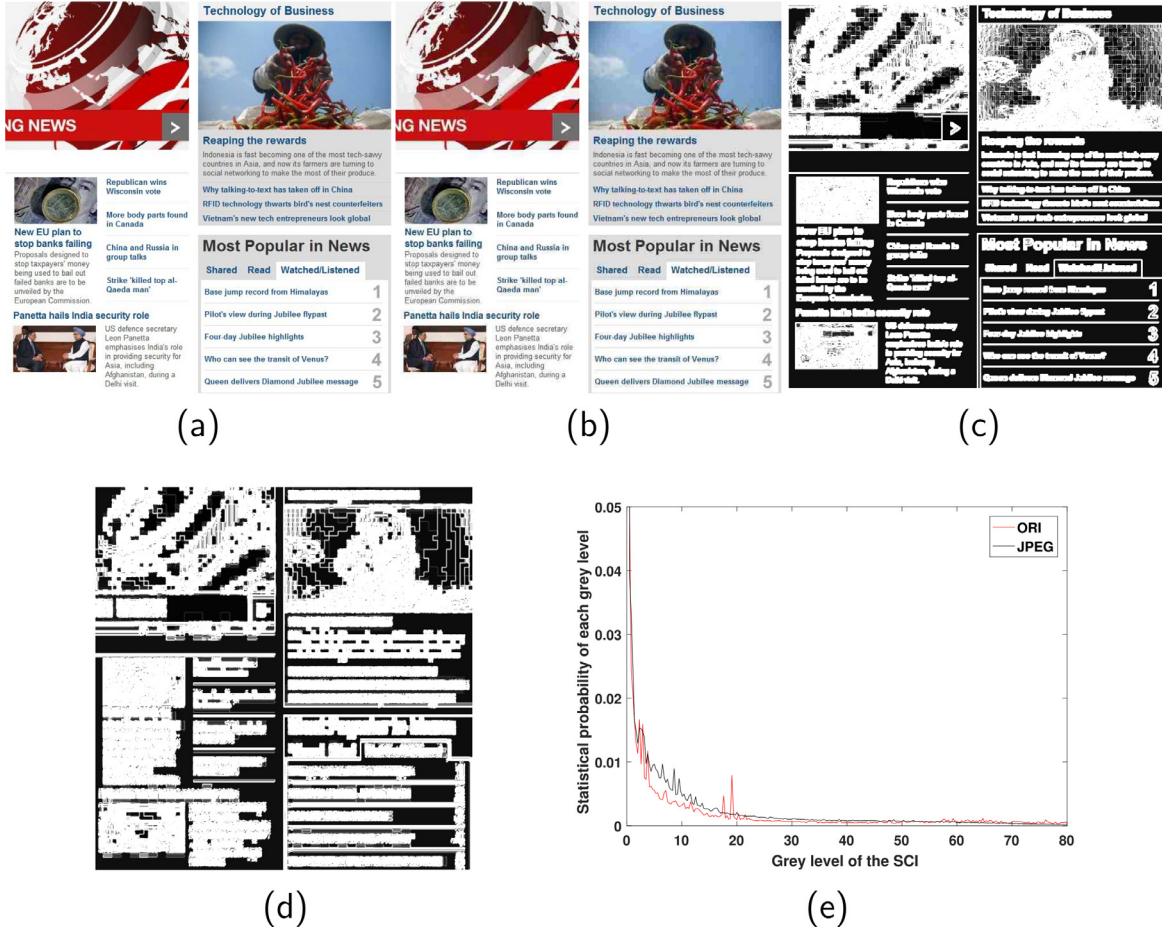


Fig. 3. The comparison of gradient magnitude between the original SCI and its JPEG distortion type. (a) an original SCI; (b) its JPEG distorted version (DMOS = 53.9965 in SIQAD database); (c) GM map of (a); (d) GM map of (b); (e) the histogram of gray level distribution in GM maps. The histogram in (e) demonstrates that distributions of the gradient magnitude in GM maps are clearly different whereas their first-order distributions are very closed.

$|F_h| + |F_v| \geq \sqrt{F_h^2 + F_v^2}$ [34]. $I(x, y)$ represents the luminance constituent of a given SCI. F_h is the horizontal derivative while F_v is vertical derivative, and they can be computed as, respectively:

$$F_h(x, y) = I(x, y) \otimes T_h. \quad (2)$$

$$F_v(x, y) = I(x, y) \otimes T_v. \quad (3)$$

where the symbol \otimes denotes the linear convolution operator. The Gaussian partial derivative filter used along the horizontal (h) or vertical (v) direction is expressed as:

$$T_\gamma(x, y|\sigma) = \frac{\partial}{\partial \gamma} g(x, y|\sigma) = -\frac{1}{2\pi\sigma^2} \frac{\gamma}{\sigma^2} \exp\left(-\frac{x^2 + y^2}{2\sigma^2}\right). \quad (4)$$

where $\gamma \in (h, v)$ and $\frac{\partial}{\partial \gamma} g(x, y|\sigma)$ is the Gaussian function with scale parameter σ . Compared with some filters (e.g. Prewitt and Robert), the Gaussian partial derivative filters can be regarded as an edge-preserving and computationally simple filter for SCIs, which is beneficial to the following computational stages, such as calculating RD and RM.

The local direction of the image is relative, and modern feature extraction mechanisms that exploit gradient direction information calculate it in a relative way, which provides more correspondent changes in local structure [42]. The relative direction (RD) can reflect the local degradation of SCI. Similarly, the relative gradient magnitude (RM) can reflect the variation of the local con-

trast. Therefore, the RD and RM respectively are expressed as:

$$F_{RD}(x, y) = \arctan \frac{\bar{F}_v(x, y)}{\bar{F}_h(x, y)}. \quad (5)$$

$$F_{RM}(x, y) = |\bar{F}_h(x, y) - F_h(x, y)| + |\bar{F}_v(x, y) - F_v(x, y)| \quad (6)$$

where \bar{F}_h and \bar{F}_v are the average directional derivative estimates in blocks of size $P \times Q$. The formula is expressed as

$$\bar{F}_\gamma(x, y) = \frac{\sum \sum F_\gamma(x-p, y-q)}{PQ}, \quad (p, q) \in \Omega. \quad (7)$$

where $\gamma \in (h, v)$, Ω is the set of the relative coordinate shift, which defines the local region through which the partial derivative values are adopted. Here we adopt the local region as 3×3 square, therefore $P = Q = 3$ (The comparison experiment is carried out with the other neighborhood sizes in Section 4.).

To verify the effectiveness of gradient maps, we show an example from a SCI chosen from the SIQAD database in Fig. 5(a). This SCI is used as a pristine image for visual quality evaluation against each corrupted SCI as demonstrated in Fig. 5(e) and (i); all the pictures are shown in the first column of Fig. 5. In order to further validate the significance of the relative gradient direction in the perceptual quality assessment for SCIs, we conduct an additional experiment on the gradient direction distribution between original SCI and its seven distortion types. As shown in Fig. 6, it is clearly observed that the visual quality degradation caused by seven distorted versions can be effectively represented by the relative gradient direction in characteristic ways, with Gaussian blur and motion

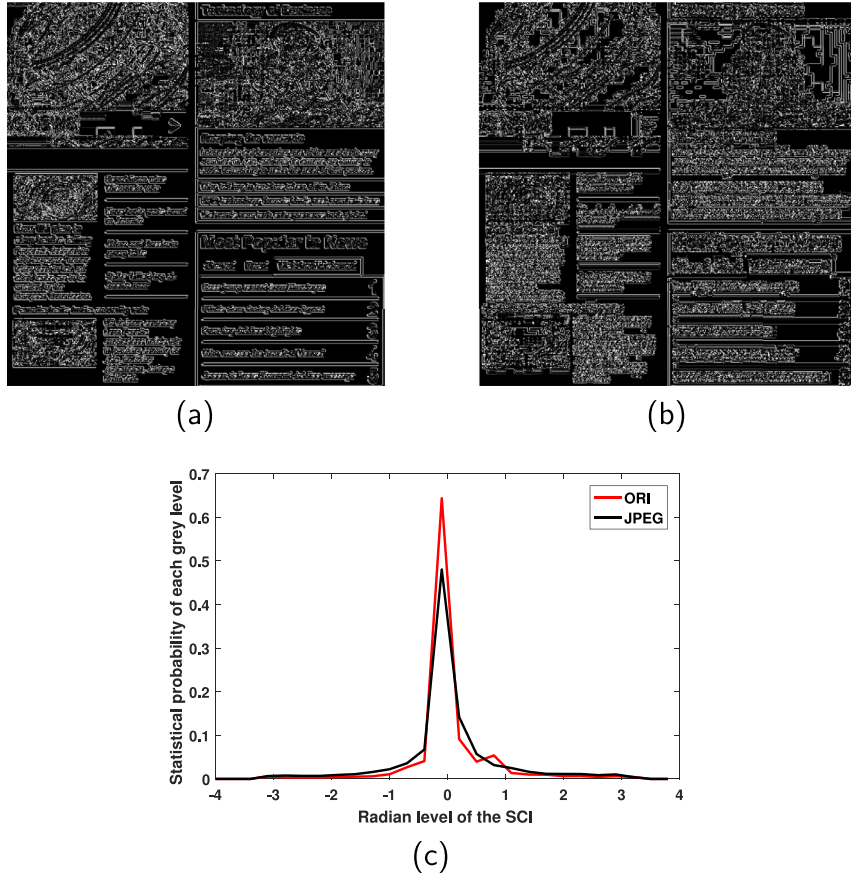


Fig. 4. The comparison of the gradient direction of original SCI and its JPEG distortion type. (a) and (b) GD maps of Fig. 3(a) and (b); (c) the histogram of radian level distribution in GD maps. The histogram in (c) demonstrates that JPEG distorted version of an original SCI can degrade its gradient directions.

blur attenuating the RD histogram. What is more, all the distortions are greatly separated in the RD histogram. Therefore, the relative gradient direction can be regarded as an important predictive factor in SCI quality evaluation.

3.3. HOG features extraction

Existing studies have shown that there is a high correlation between the derivative information of different orders and texture features of images [44]. The first-order gradient information is connected with the slope and the elasticity, which partially characterize the geometric properties of a landscape, whereas the second-order gradient information captures the curvature in relation with geometric properties of the neural landscape [44]. There are plenty of words in the textual part and the high-frequency image in pictorial part in SCI, where texture information can well be captured by different distorted versions. Thus the second-order gradient derivative information can effectually capture the changes in minor local structures that influence the perceptive degradation of SCIs [27].

The HOG descriptor [45] is consisted of the gradient direction histogram of the local region of an image, which is widely applied in pedestrian detection [46]. The basic theory behind the HOG descriptor is that the appearance and shape of the local objects within an image can be characterized according to intensity of gradients or distributions of edge directions. Here HOG features extracted from gradient maps as aforementioned are represented as texture information of SCIs by the second-order gradient derivative. Before HOG features are extracted, the image is required to be normalized in order to reduce the effect of illumination. In this pa-

per, the gamma correction is used which is expressed as:

$$F(x, y) = |F(x, y)|^\gamma \quad (8)$$

where $\gamma = 0.5$, and (x, y) is the location of the pixel. Next the image should be divided into several blocks with several cells to calculate the image gradient in different directions. Similarly as the stage before, the gradient direction $Dir(x, y)$ modified is computed as

$$\theta(x, y) = \arctan\left(\frac{F_v(x, y)}{F_h(x, y)}\right) \quad (9)$$

$$Dir(x, y) = \begin{cases} \theta(x, y) + \pi, & \theta(x, y) < 0 \\ \theta(x, y), & \theta(x, y) \geq 0 \end{cases} \quad (10)$$

Then a cell unit is consisted of a block involving 8×8 pixels and we divide the gradient direction of each block into 9 different regions, where each direction interval is 40° . Therefore, there are 9 HOG features in corresponding 9° intervals for each cell. Because of the variation of local illumination and the contrast between foreground and background, the range of gradient intensity is very large. So normalization of the gradient intensity is required in processing, which further compresses light, shadows and edges. Each cell unit is combined into a large and spatially connected block, which is normalized by Eq. (10):

$$f_{h-N} = \frac{f_h}{\|f_h\|_2 + C} \quad (11)$$

where f_h represents the corresponding HOG feature in each degree interval and N indicates the normalization process; the symbol $\|\cdot\|_2$ denotes the L_2 norm and C represents a positive constant



Fig. 5. An example of gradient magnitude map (GM), relative gradient direction map (RD) and relative gradient magnitude map (RM) of the test SCI and its two types of distorted versions. [Column 1]: (a) a pristine or reference SCI; (e) a distorted SCI corrupted by motion blur; (i) a distorted SCI corrupted by JPEG compression. [Columns 2–4]: their corresponding GM map, RD map, and RM map, respectively.

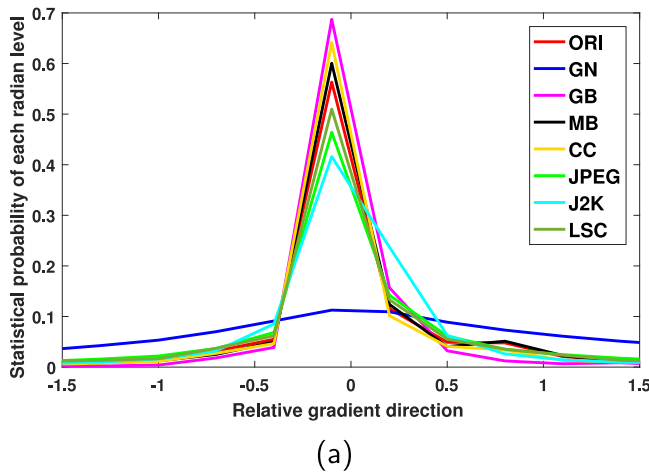


Fig. 6. Histogram of relative gradient direction maps of the original SCI in Fig. 5(a) and its seven corresponding distorted versions.

in case of the denominator becomes 0. Here 2×2 cell units are employed as one block and therefore there are 36 HOG features for each block in the image. Finally the average value of all blocks is adopted as the corresponding HOG feature, which can be com-

puted as:

$$f_{hi} = \frac{1}{n_B} \sum_{j=1}^{n_B} f_{hi-N,j}, \quad (h_i = 1, 2, 3, \dots, 36) \quad (12)$$

where f_{hi} represents the HOG feature in each degree interval of every cell unit and n_B denotes the quantity of blocks in each test image. Thus 108 HOG features are extracted from three types of gradient maps. Multiscale theory is widely used in feature extraction, which is determined by physical and psychological vision. Therefore, images are resized by down-sampling with factors of 2. Finally there are totally 216 features for each corrupted SCI.

3.4. Dictionary learning

The construction of the dictionary plays an important role in the sparse representation of signals. For the training set of SCIs, texture features are extracted from the SCIs firstly. Assuming that the training set has n SCIs, the texture feature \mathbf{f}_i extracted from each SCI is a 216×1 dimensional feature vector. So the n SCIs have a feature matrix of $216 \times n$ dimensions:

$$\mathbf{G} = [\mathbf{f}_1, \mathbf{f}_2, \mathbf{f}_3, \dots, \mathbf{f}_n] \quad (13)$$

Each SCI in the training set corresponds to a $dmos$ value. N $dmos$ values in the training set are combined to obtain an n -dimensional

DMOS' vector:

$$\mathbf{DMOS}' = [dmos_1', dmos_2', dmos_3', \dots, dmos_n'] \quad (14)$$

The feature matrix \mathbf{G} and \mathbf{DMOS}' of the training set are integrated, and a dictionary \mathbf{H} of the training set is constructed:

$$\mathbf{H} = \begin{bmatrix} \mathbf{G} \\ \mathbf{DMOS}' \end{bmatrix} \doteq \begin{bmatrix} \mathbf{f}_1 & \mathbf{f}_2 & \dots, & \mathbf{f}_n \\ dmos_1', dmos_2', \dots, dmos_n' \end{bmatrix} \quad (15)$$

where the symbol \doteq represents that the dictionary is constructed by feature matrix \mathbf{G} and vector \mathbf{DMOS}' . \mathbf{G} denotes an $m \times n$ feature matrix ($m = 216$ and n represents the quantity of training SCIs). Vector \mathbf{DMOS}' denotes the corresponding *dmos* values of the training SCIs.

3.5. Sparse representation

Existing studies about HVS prove that human visual perception has an important characteristic of sparsity [47]. The aim of the sparse representation is to represent some of the particular structures in the atom via a compact form, and the majority of information in the signal can be represented by a small number of atomic signals. Sparse representation can effectively and reasonably select a small number of training samples to achieve the optimal representation of image features. Therefore, it can reduce the disturbance of SCIs with great differences of perceptive quality in the designed model. In the test set phase, we find sparse representation coefficients of the extracted 216-dimensional feature vector in the dictionary \mathbf{H} (The dimension is $217 \times n$). It can be expressed as:

$$y = \sum_{i=1}^n \alpha_i \mathbf{H}_i \quad (16)$$

where α_i (The dimension is 1×217) represents the coefficients of each feature vector in the training SCI and \mathbf{H}_i is the i th column in the dictionary \mathbf{H} . If we multiply the coefficients vector with the dictionary, the upper expression can be simplified to Eq. (17).

$$y = \sum_{i=1}^n \alpha_i \mathbf{H}_i = \mathbf{H}\alpha \quad (17)$$

where α is expressed as the sparse coefficients vector closest to the sparse representation of feature vector in the test SCI, whose sparse representation coefficients can be obtained by sparse representation in the dictionary \mathbf{H} :

$$\alpha^* = \arg \min_{\alpha \in \mathbb{R}^N} \|\alpha\|_0 \quad \text{s.t. } y = \mathbf{H}\alpha \quad (18)$$

where \mathbb{R}^N is n -dimensional real-number space and s.t. is expressed as under a given condition. Because the l_0 -minimization is regarded as an NP-hard problem in general [48], the best solution by using l_1 -minimization is usually exploited [49]. Next this formula can be translated into as follows:

$$\alpha^* = \arg \min_{\alpha \in \mathbb{R}^N} \|\alpha\|_1 \quad \text{s.t. } y = \mathbf{H}\alpha \quad (19)$$



Fig. 7. The predictive scores of three types of distorted SCIs. (a) Gaussian noise, DMOS = 42.77; (b) Gaussian blur, DMOS = 77.89; JPEG compression, DMOS = 58.30.

This question can next be simplified as an unconstrained optimization question

$$\alpha^* = \arg \min_{\alpha \in \mathbb{R}^N} \lambda \|\alpha\|_1 + \|y - \mathbf{H}\alpha\|_2 \quad (20)$$

here the parameter λ denotes a positive constant in order to balance the fidelity term and the sparse regularization term. Finally the least absolute shrinkage and selection operator is exploited to solve the unconstrained convex optimization problems [50].

3.6. Quality pooling

Through the above procedures, the sparse coefficients vector α^* of f in the dictionary is gained. In accordance with the assumption that if SCIs have the same subjective quality scores their features will have identical distributions, the visual quality of the test SCI can be pooled by the *dmos'* value of the training SCIs, i.e.,

$$Q = \frac{\sum_{i=1}^n \alpha_i^* dmos'_i}{\sum_{i=1}^n \alpha_i^*} \quad (21)$$

where $dmos'_i$ denotes the DMOS values of the i th SCI in the dictionary \mathbf{H} . The prediction Q , which ranges from 0 to 100, is the output quality score of the test SCI, and a smaller value of Q indicates a higher perceptive quality of the test SCI. Several examples be given for various corruptions of SCIs in Fig. 7.

4. Experimental results

4.1. Screen content image database

The Screen Image Quality Assessment Database (SIQAD) [51] will be applied to test the superiority of the designed model. So far as we know, the first SIQAD database is consisted of 980 distorted SCIs, which are provided by corrupting 20 reference SCIs. There are 7 kinds of distorted versions with 7 degradation levels in a reference image. Seven distorted versions, containing Gaussian noise (GN), Gaussian blur (GB), motion blur (MB), contrast change (CC), JPEG compression (JPEG), JPEG2000 compression (J2K) and layer segmentation-based Coding (LSC) [52], are utilized to each of the pristine SCIs. These 20 pristine SCIs are obtained from digital magazines, PowerPoint files and Internet pages via screen snapshots. Because the subjective test of the SIQAD database is carried out by computer, the image size can be adjusted according to a certain resolution to display on the computer. Some examples of SCIs in the SIQAD database are provided in Fig. 8.

We also employ one more SCI database. The screen content image database (SCID) [34] consists of 40 original SCIs and 1800 distortion types provided from these reference SCIs. Nine kinds of distorted versions include: the Gaussian noise (GN), the Gaussian blur (GB), and motion blur (MB), contrast change (CC), color quantization with dithering (CQD), JPEG and JPEG2000 (J2K), high efficiency video coding (HEVC) and screen content coding (SCC).

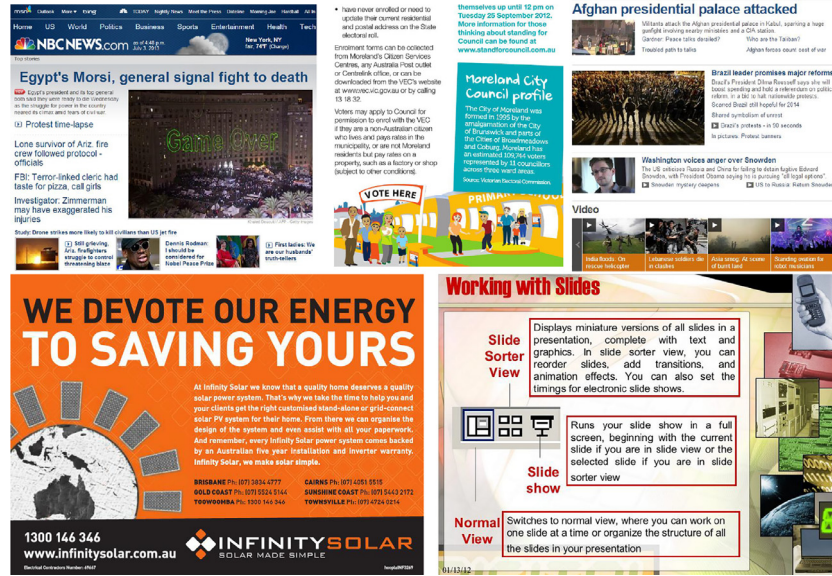


Fig. 8. Some examples of SCIs in SIQAD.

4.2. Performance measures

In order to validate the effective of the designed algorithm, we use three typically-exploited performance approaches: *Pearson Linear Correlation Coefficient* (PLCC), *Spearman Rank-order Correlation Coefficient* (SRCC), and *Root Mean Square Error* (RMSE). SRCC is directly calculated by subjective scores and objective scores while the rest two are calculated after a regression process. The five-parameters logistic mapping function [53] is employed and represented as:

$$r_x = \beta_1 \cdot \left[\frac{1}{2} - \frac{1}{1 + \exp(\beta_2 \cdot (x - \beta_3))} \right] + \beta_4 \cdot x + \beta_5 \quad (22)$$

where x and r_x represent subjective scores and object scores of an objective IQA model respectively. In addition, a lower RMSE value demonstrates a better performance while higher values of PLCC and SRCC indicate a superior result. The functions 'nlfit' and 'nlpredci' of MATLAB fit the curve and determinate five-parameters' values in the nonlinear regression model. The PLCC value is calculated for the prediction accuracy while the SRCC value is computed for the prediction monotonicity. The RMSE value can be exploited to estimate the prediction consistency. Of the three indices introduced above, a value close to 1 for the PLCC value and the SRCC value, and near to 0 for the RMSE value represent the better correlation with human eye perception.

Table 1
The experimental PLCC results of the designed method compared with several schemes in the SIQAD database.

Indices		GN	GB	MB	CC	JPEG	J2K	LSC	ALL
FR models	PSNR	0.9053	0.8603	0.7044	0.7401	0.7545	0.7893	0.7805	0.5869
	SSIM [4]	0.8806	0.9014	0.8060	0.7435	0.7487	0.7749	0.7307	0.7561
	MSSIM [5]	0.8783	0.8984	0.8240	0.8371	0.7756	0.7951	0.7729	0.6161
	FSIM [6]	0.7428	0.7206	0.6874	0.7507	0.5566	0.6675	0.6964	0.5389
	SIQM [29]	0.892	0.912	0.845	0.790	0.771	0.794	0.720	0.852
	ESIM [34]	0.8891	0.9234	0.8886	0.7641	0.7999	0.7888	0.7915	0.8788
NR models	NIQE [14]	0.8045	0.4799	0.2012	0.3132	0.4268	0.1849	0.4177	0.3415
	BRISQUE [13]	0.8376	0.8359	0.7666	0.5489	0.7346	0.7645	0.6980	0.7237
	QAC [17]	0.8525	0.5587	0.3780	0.0744	0.3017	0.1885	0.3367	0.3751
	BLIQUP- SCI [37]	0.9015	0.9453	0.6341	0.7278	0.6691	0.6001	0.4253	0.7705
	NRLT [27]	0.9131	0.8949	0.8993	0.8131	0.7932	0.6848	0.7228	0.8442
	Proposed	0.9291	0.9367	0.9243	0.6563	0.8334	0.8347	0.8069	0.8618

4.3. Overall performance in the SIQAD database

To verify the superiority of the designed metric, we choose some traditional and representative schemes as comparison in the SIQAD database, including six full-reference models (PSNR, SSIM [4], MS-SSIM [5], FSIM [6], SIQM [29], ESIM [34]), and five no-reference models (NIQE [14], BRISQUE [13], QAC [17], BLIQUP-SCI [37], NRLT [27]). What is more, SIQM, ESIM, BLIQUP-SCI and NRLT are particularly proposed for the perceptive quality assessment of SCIs whereas the remainders are all for evaluating natural images.

Tables 1–3 demonstrate the PLCC, SRCC, and RMSE results of the designed scheme and other algorithms employing the test SCIs selected from the SIQAD database, respectively. The highest three experimental results of each predictive index (i.e., PLCC, SRCC, and RMSE) are emphasized in boldface, and the highest one is further emphasize in red color in order to easy comparison. For these methods, the results of all metrics are taken from the originally published papers. What is more, the experimental results conducted on each distorted version are also listed besides the RMSE values of QAC, BLIQUP-SCI and NRLT, which is because the result and source program are not provided. Since no reference metrics and the proposed model require distorted SCIs to train the regression model, SCI samples in the SIQAD database are randomly divided into two parts. Specifically, the first part includes 80% SCI samples which are applied for training and the rest 20% image samples are applied for testing. To validate the robust of experi-

Table 2

The experimental SRCC results of the designed method compared with several schemes in the SIQAD database.

Indices		GN	GB	MB	CC	JPEG	J2K	LSC	ALL
FR models	PSNR	0.8790	0.8573	0.7130	0.6828	0.7569	0.7746	0.7930	0.5604
	SSIM [4]	0.8694	0.8921	0.8041	0.6405	0.7565	0.7749	0.7307	0.7566
	MSSIM [5]	0.8679	0.8883	0.8238	0.7506	0.7787	0.7855	0.7711	0.6165
	FSIM [6]	0.7373	0.7286	0.6641	0.7175	0.5879	0.6363	0.5979	0.5279
	SIQM [29]	0.871	0.910	0.840	0.705	0.775	0.777	0.725	0.845
	ESIM [34]	0.8757	0.9239	0.8938	0.6108	0.7989	0.7827	0.7958	0.8632
NR models	NIQE [14]	0.8242	0.5668	0.3753	0.0690	0.4474	0.2467	0.3441	0.3695
	BRISQUE [13]	0.8665	0.8234	0.6786	0.7256	0.7543	0.7456	0.6323	0.7708
	QAC [17]	0.8416	0.6238	0.3375	0.0745	0.1451	0.1937	0.1866	0.3009
	BLIQUP-SCI [37]	0.8208	0.8320	0.7004	0.4920	0.6562	0.5873	0.4144	0.7990
	NRLT [27]	0.8966	0.8812	0.8919	0.7072	0.7698	0.6761	0.6978	0.8202
	Proposed	0.9144	0.9311	0.9148	0.6498	0.8377	0.8354	0.7948	0.8354

Table 3

The experimental RMSE results of the designed method compared with several schemes in the SIQAD database.

Indices		GN	GB	MB	CC	JPEG	J2K	LSC	ALL
FR models	PSNR	6.3372	7.7376	9.2287	8.4591	6.1665	6.3819	5.3386	11.5898
	SSIM [4]	7.0679	6.5701	7.6979	8.4116	6.2295	6.5691	5.8253	9.3676
	MSSIM [5]	7.1309	6.6638	7.3675	6.8818	5.9311	6.3040	5.4141	11.2744
	FSIM [6]	9.9860	10.5203	9.4432	8.3190	7.8072	7.7402	6.8486	12.0583
	SIQM [29]	7.0165	5.8367	6.0869	8.0179	5.6548	6.0820	5.3576	7.4936
	ESIM [34]	6.8278	5.8270	5.9639	8.1141	5.6401	6.3877	5.2150	6.8310
NR models	NIQE [14]	8.5645	7.9880	10.676	10.042	8.7865	8.4532	7.8774	13.4670
	BRISQUE [13]	7.5643	8.4593	9.4532	8.6786	5.8643	6.1375	6.2321	8.2565
	QAC [17]	—	—	—	—	—	—	—	13.269
	BLIQUP-SCI [37]	—	—	—	—	—	—	—	10.020
	NRLT [27]	—	—	—	—	—	—	—	5.6217
	Proposed	5.3105	5.2141	5.5266	10.5005	5.2541	5.6377	5.6217	7.4910

mental performance, the above procedure is randomly conducted 1000 iterations and the median values across the 1000 times are documented.

As shown in Tables 1–3, it can be concluded that the designed metric has the superiority over other models (e.g., NR methods and most FR methods) under comparison besides the full reference ESIM model, but ours is the closest to it. It proves that the proposed metric have the high consistency and accuracy with the human visual perception. Note that all metrics particularly developed for the visual quality evaluation of SCI (i.e., SIQM, ESIM, BLIQUP-SCI, NRLT) and the designed algorithm can have the better superior results than those classical IQA metrics proposed for natural images in the SIQAD database. It is mostly because they considered the particularity of SCIs when designing perceptive quality assessment model for SCIs.

In order to comprehensively assess the three types of indices to predict the quality degradations of SCIs caused by different distorted versions, we conduct the performance experiment of the proposed metric and other classical algorithms on seven types of distortion versions. Tables 1–3 list the experimental results. For each distorted version, the proposed model has the highest superiority over most of distortion types. What is more, it can be obviously observed that the proposed scheme can more precisely evaluate and reflect the degenerations distorted by Gaussian noise (GN), Gaussian blur (GB), motion blur (MB), JPEG compression and JPEG2000 compression especially. It is expected because blurring and compression distorted versions can degenerate the texture structure of SCI, and texture features extracted can be significantly changed. Although the proposed method can have the satisfactory experimental results, poor performance results are obtained on Contrast change (CC). The reason is mainly that image intensity rather than the texture of the image is modified by the CC distortion. Moreover, scatter plots between of the objective predict quality scores against the DMOS values in all and each distortion type of the SIQAD database are, respectively, shown in Fig. 9. Clearly, the

Table 4

The comparison performance in the SCID database.

ModelS	PLCC	SRCC	RMSE
PSNR	0.7622	0.7512	9.1682
SSIM [4]	0.7343	0.7146	9.6133
MSSIM [5]	0.7579	0.7407	9.2400
FSIM [6]	0.7719	0.7550	9.0040
SIQM [29]	0.7766	0.7590	9.3854
NRLT [27]	0.6625	0.6454	10.6452
Proposed	0.8017	0.7840	8.8041

Table 5

The comparison performance with different gradient maps.

Indices	GM	RD	RM	ALL
PLCC	0.8021	0.8269	0.8174	0.8618
SRCC	0.7702	0.7989	0.7793	0.8360
RMSE	8.5902	8.1661	8.3193	7.2236

proposed metric has better convergence across different distortion types, which further demonstrates the robustness and effectiveness of the model.

Additionally, Table 4 lists the experimental results of the designed model in contrast to six types of natural image quality evaluation algorithms in the SCID database and the highest value is bolded. According to this table, it can be obviously observed that the designed metric holds the best performance and shows a stronger robustness in assessing the perceptive quality of SCIs in the SCID database.

4.4. Comparison results on individual gradient maps

In this subsection, the comparison experiment is conducted to validate the superiority using each gradient map on the SIQAD database. As shown in Table 5, it is clearly demonstrated that the

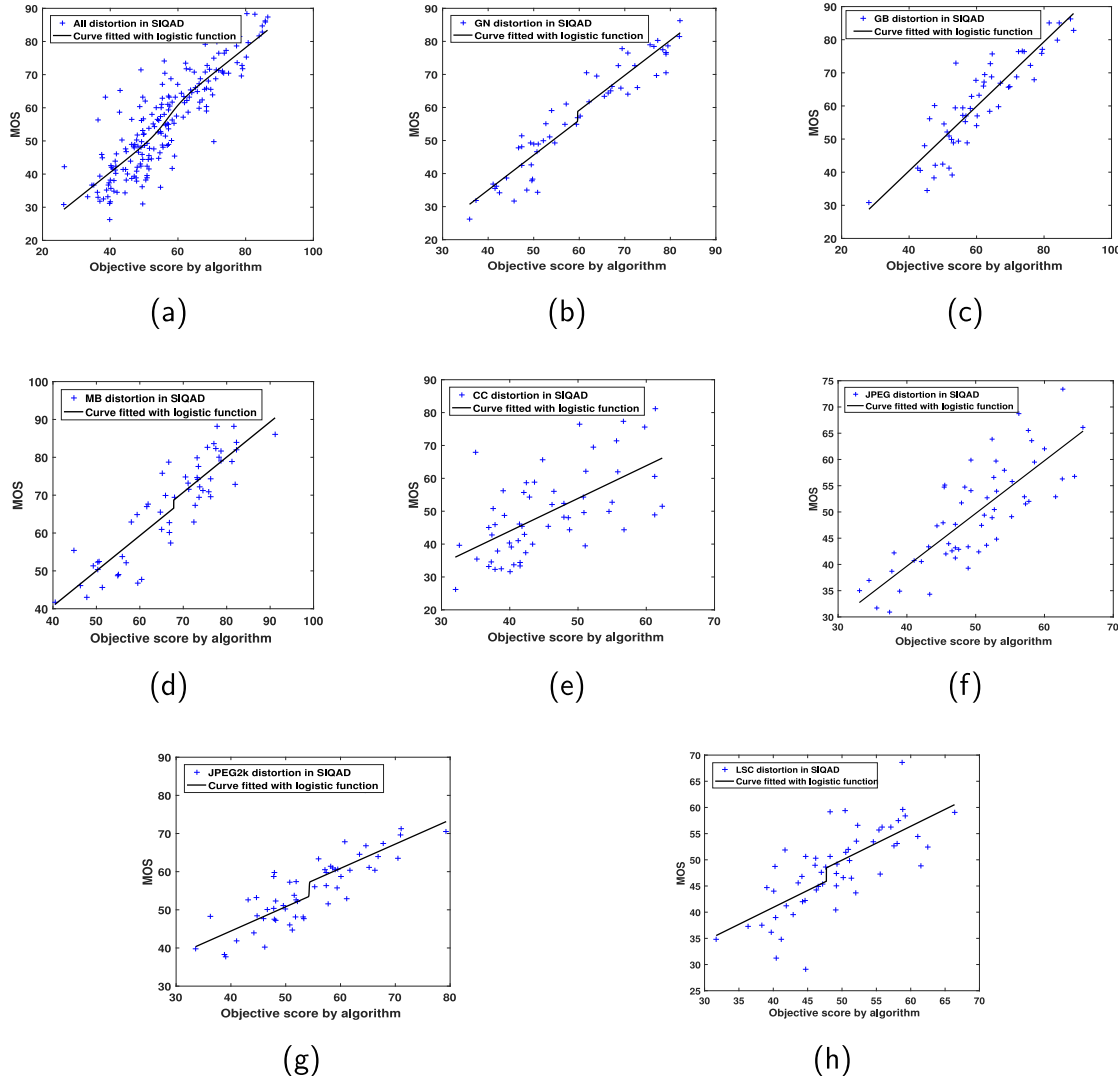


Fig. 9. The scatter plots of predicted quality scores by different distortions against the DMOS values in the SIQAD database. (a) All distortion types (b) Gaussian noise (c) Gaussian blurring (d) Motion blurring (e) Contrast change (f) JPEG compression (g) JPEG2K compression (h) Layer-segmentation based compression.

designed algorithm using RD map can obtain the highest experimental results than that using the GM map and the RM map respectively because the relative gradient direction provides structural information that is complementary to that provided by the absolute gradient magnitude. Meanwhile, the performance using the GM map is the worst, which indicates the mode of measurement in a relative manner is better. Overall, the proposed method using all gradient maps can achieve the highest superiority than that using only one type of gradient map.

4.5. Comparison results with SVR

To demonstrate the effectiveness of sparse representation in our proposed metric, we also conducted the comparison experiment with the model using SVR in the SIQAD database. What is more, an additional ablation study is made to verify the usefulness of an optimal weight vector α . Here a uniform weight weights are used as α . As shown in the Table 6, it is obviously observed that indicators using SVR are lower than the metric using sparse representation. This is mainly because sparse representation is a simulation of the encoding mechanism of human cerebral cortex, and SVR cannot abstract and optimize extracted features. Therefore, the

Table 6

The comparison performance between using SVR and using sparse representation.

Indices	PLCC	SRCC	RMSE
SVR	0.8441	0.8119	7.8949
Sparse representation (uniform weights)	0.8532	0.8276	7.7452
Sparse representation (optimized weights)	0.8618	0.8360	7.2256

metric using sparse representation is more consistent with the HVS and can have the better predictive performance for SCIs.

4.6. Parameter setting

In this subsection, comparison experiment is conducted to validate the influence of the parameter setting in the SIQAD database. Fig. 10 demonstrates the experimental results with the sizes of the different windows in the process that gradient quantities are calculated. It can be concluded that the indices are higher with smaller window size, since the texture feature computed is highly sensitive to the local distortion. Therefore, the size of the window is set to 3*3. The quality-aware features with different quantity of scales

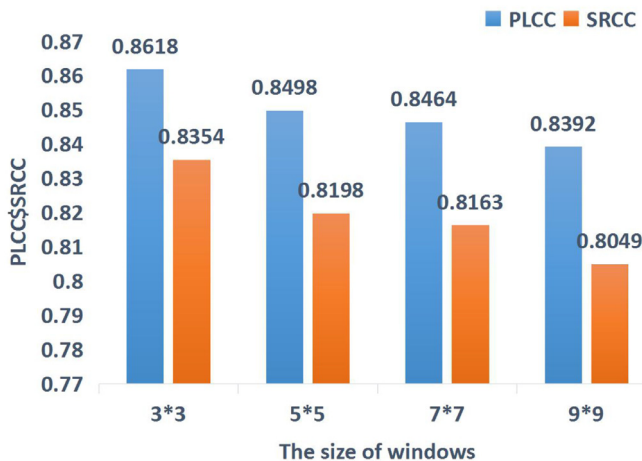


Fig. 10. The comparison performance with different sizes of window in terms of PLCC and SRCC.

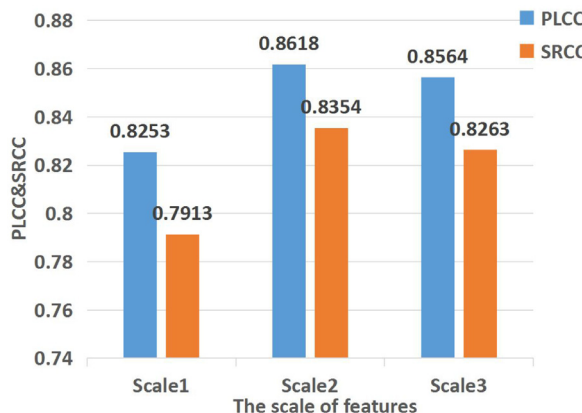


Fig. 11. The comparison performance with different scales of feature extraction in terms of PLCC and SRCC.

are extracted for feature representation. The performance figures are demonstrated in Fig. 11, from which it can be observed that there is no better performance in the perceptive quality evaluation of SCIs when the quantity of scales is more than two. Thus, the quantity of scales is set to two.

5. Conclusion

In this paper, a hot research problem—screen content IQA has been studied and a no-reference quantitative measure via modeling image gradients based on sparse representation has been proposed. The proposed model extracts HOG features from first-order gradient information representing texture features as second-order derivatives. After the features are extracted, it is composed of two important procedures: representing HOG features by means of sparse coding, then weighting subjective experimental quality scores via the sparse coding coefficients to predict objective perceptive quality scores of SCIs. Experimental performance proves that the designed scheme can have better superiority, including even some full reference visual quality evaluation algorithms. In future work, the accurate segmentation of pictorial part and textual part in the distorted screen content image will be considered.

Acknowledgments

This work was partially supported by National Natural Science Foundation of China (No. 61471260), Natural Science Foundation of Tianjin City (No. 16JCYBJC16000) and Foundation of Pre-Research on Equipment of China (No. 61403120103).

References

- [1] W. Xue, L. Zhang, X. Mou, A.C. Bovik, Gradient magnitude similarity deviation: a highly efficient perceptual image quality index, *IEEE Trans. Image Process.* 23 (2) (2014) 95–684.
- [2] R. Hong, L. Zhang, D. Tao, Unified photo enhancement by discovering aesthetic communities from flickr, *IEEE Trans. Image Process.* 25 (3) (2016) 1124–1135.
- [3] R. Hong, Y. Yang, M. Wang, X.S. Hua, Learning visual semantic relationships for efficient visual retrieval, *IEEE Trans. Big Data* 1 (4) (2017) 152–161.
- [4] Z. Wang, A.C. Bovik, H.R. Sheikh, E.P. Simoncelli, Image quality assessment: from error visibility to structural similarity, *IEEE Trans. Image Process.* 13 (4) (2004) 600.
- [5] Z. Wang, E.P. Simoncelli, A.C. Bovik, Multiscale structural similarity for image quality assessment, in: Proceedings of the 2004 Conference Record of the Thirty-Seventh Asilomar Conference on Signals, Systems and Computers, 2004, pp. 1398–1402. Vol.2.
- [6] L. Zhang, L. Zhang, X. Mou, D. Zhang, FSIM: a feature similarity index for image quality assessment, *IEEE Trans. Image Process. Publ. IEEE Signal Process. Soc.* 20 (8) (2011) 2378–2386.
- [7] H.R. Sheikh, A.C. Bovik, Image information and visual quality, *IEEE Trans. Image Process. Publ. IEEE Signal Process. Soc.* 15 (2) (2006) 430.
- [8] J. Wu, W. Lin, G. Shi, A. Liu, Perceptual quality metric with internal generative mechanism, *IEEE Trans. Image Process. Publ. IEEE Signal Process. Soc.* 22 (1) (2013) 43.
- [9] L. Zhang, Y. Shen, H. Li, VSI: a visual saliency-induced index for perceptual image quality assessment, *IEEE Trans. Image Process.* 23 (10) (2014) 4270–4281.
- [10] Y. Wang, T. Jiang, S. Ma, W. Gao, Image quality assessment based on local orientation distributions, in: Proceedings of the 2011 Picture Coding Symposium, 2011, pp. 274–277.
- [11] Y. Yang, D. Tu, G. Cheng, Image quality assessment using histograms of oriented gradients, in: Proceedings of the Fourth International Conference on Intelligent Control and Information Processing, 2013, pp. 555–559.
- [12] A.K. Moorthy, A.C. Bovik, Blind image quality assessment: from natural scene statistics to perceptual quality, *IEEE Trans. Image Process. Publ. IEEE Signal Process. Soc.* 20 (12) (2011) 3350.
- [13] A. Mittal, A.K. Moorthy, A.C. Bovik, No-reference image quality assessment in the spatial domain, *IEEE Trans. Image Process.* 21 (12) (2012) 4695.
- [14] A. Mittal, R. Soundararajan, A.C. Bovik, Making a completely blind image quality analyzer, *IEEE Signal Process. Lett.* 20 (3) (2013) 209–212.
- [15] L. Zhang, L. Zhang, A.C. Bovik, A feature-enriched completely blind image quality evaluator, *IEEE Trans. Image Process.* 24 (8) (2015) 2579–2591.
- [16] M.A. Saad, A.C. Bovik, C. Charrier, Blind image quality assessment: a natural scene statistics approach in the DCT domain, *IEEE Trans. Image Process.* 21 (8) (2012) 3339.
- [17] W. Xue, L. Zhang, X. Mou, Learning without human scores for blind image quality assessment, in: Proceedings of the 2013 Computer Vision and Pattern Recognition, 2013, pp. 995–1002.
- [18] Z. Shi, J. Zhang, Q. Cao, K. Pang, T. Luo, Full-reference image quality assessment based on image segmentation with edge feature, *Signal Process.* 145 (2017).
- [19] R. Hong, J. Pan, S. Hao, M. Wang, F. Xue, X. Wu, Image quality assessment based on matching pursuit, *Inf. Sci. (NY)* 273 (3) (2014) 196–211.
- [20] W. Hou, X. Gao, D. Tao, X. Li, Blind image quality assessment via deep learning, *IEEE Trans. Neural Netw. Learn. Syst.* 26 (6) (2017) 1275–1286.
- [21] J. Kim, S. Lee, Deep learning of human visual sensitivity in image quality assessment framework, in: Proceedings of the 2017 IEEE Conference on Computer Vision and Pattern Recognition, 2017, pp. 1969–1977.
- [22] Z. Wang, G. Wu, H.R. Sheikh, E.P. Simoncelli, E.H. Yang, A.C. Bovik, Quality-aware images., *IEEE Trans. Image Process.* 15 (6) (2006) 1680–1689.
- [23] A. Rehman, Z. Wang, Reduced-reference image quality assessment by structural similarity estimation, *IEEE Trans. Image Process. Publ. IEEE Signal Process. Soc.* 21 (8) (2012) 3378–3389.
- [24] G. Zhai, X. Wu, X. Yang, W. Lin, W. Zhang, A psychovisual quality metric in free-energy principle, *IEEE Trans. Image Process. Publ. IEEE Signal Process. Soc.* 21 (1) (2012) 41.
- [25] Y. Xu, D. Liu, Y. Quan, C.P. Le, Fractal analysis for reduced reference image quality assessment, *IEEE Trans. Image Process.* 24 (7) (2015) 2098.
- [26] Y. Liu, G. Zhai, K. Gu, X. Liu, D. Zhao, W. Gao, Reduced-reference image quality assessment in free-energy principle and sparse representation, *IEEE Trans. Multimed. PP* (99) (2017) 1–1.
- [27] Y. Fang, J. Yan, L. Li, J. Wu, W. Lin, No reference quality assessment for screen content images with both local and global feature representation, *IEEE Trans. Image Process. PP* (99) (2018) 1–1.
- [28] H. Yang, Y. Fang, W. Lin, Perceptual quality assessment of screen content images, *IEEE Trans. Image Process.* 24 (11) (2015) 4408–4421.
- [29] K. Gu, S. Wang, G. Hai, S. Ma, W. Lin, Screen image quality assessment incorporating structural degradation measurement, in: Proceedings of the 2015 IEEE International Symposium on Circuits and Systems, 2015, pp. 125–128.

- [30] S. Wang, K. Gu, K. Zeng, Z. Wang, W. Lin, Objective quality assessment and perceptual compression of screen content images, *IEEE Comput. Graph. Appl.* PP (99) (2016) 47–58.
- [31] K. Gu, S. Wang, H. Yang, W. Lin, G. Zhai, X. Yang, W. Zhang, Saliency-guided quality assessment of screen content images, *IEEE Trans. Multimed.* 18 (6) (2016) 1098–1110.
- [32] S. Wang, K. Gu, X. Zhang, W. Lin, S. Ma, W. Gao, Reduced-reference quality assessment of screen content images, *IEEE Trans. Circuits Syst. Video Technol.* PP (99) (2016) 1–1.
- [33] L. Zuo, H. Wang, J. Fu, Screen content image quality assessment via convolutional neural network, in: Proceedings of the 2016 IEEE International Conference on Image Processing, 2016, pp. 2082–2086.
- [34] Z. Ni, L. Ma, H. Zeng, J. Chen, C. Cai, K.K. Ma, ESIM: edge similarity for screen content image quality assessment, *IEEE Trans. Image Process. Publ. IEEE Signal Process. Soc.* PP (99) (2017) 4818–4831.
- [35] Y. Fang, J. Yan, J. Liu, S. Wang, Q. Li, Z. Guo, Objective quality assessment of screen content images by uncertainty weighting, *IEEE Trans. Image Process. Publ. IEEE Signal Process. Soc.* 26 (4) (2017) 2016–2027.
- [36] S. Wang, K. Gu, X. Zhang, W. Lin, L. Zhang, S. Ma, W. Gao, Subjective and objective quality assessment of compressed screen content images, *IEEE J. Emerging Sel. Top. Circuits Syst.* 6 (4) (2017) 532–543.
- [37] F. Shao, Y. Gao, F. Li, G. Jiang, Toward a blind quality predictor for screen content images, *IEEE Trans. Syst. Man Cybern. Syst. PP* (99) (2017) 1–10.
- [38] K. Gu, J. Zhou, J.F. Qiao, G. Zhai, W. Lin, A.C. Bovik, No-reference quality assessment of screen content pictures, *IEEE Trans. Image Process.* 26 (8) (2017) 4005–4018.
- [39] N. Lu, G. Li, Blind quality assessment for screen content images by orientation selectivity mechanism, *Signal Process.* 145 (2017).
- [40] A. Liu, W. Lin, M. Narwaria, Image quality assessment based on gradient similarity, *IEEE Trans. Image Process.* 21 (4) (2012) 1500–1512.
- [41] W. Xue, X. Mou, L. Zhang, A.C. Bovik, X. Feng, Blind image quality assessment using joint statistics of gradient magnitude and Laplacian features., *IEEE Trans. Image Process.* 23 (11) (2014) 4850–4862.
- [42] L. Liu, Y. Hua, Q. Zhao, H. Huang, A.C. Bovik, Blind image quality assessment by relative gradient statistics and adaboosting neural network, *Signal Process. Image Commun.* 40 (C) (2016) 1–15.
- [43] Z. Ni, L. Ma, H. Zeng, C. Cai, K.K. Ma, Gradient direction for screen content image quality assessment, *IEEE Signal Process. Lett.* 23 (10) (2016) 1394–1398.
- [44] D. Huang, C. Zhu, Y. Wang, L. Chen, HSOG: a novel local image descriptor based on histograms of the second-order gradients, *IEEE Trans. Image Process. Publ. IEEE Signal Process. Soc.* 23 (11) (2014) 4680.
- [45] O. Déniz, G. Bueno, J. Salido, Face recognition using Histograms of Oriented Gradients, *Pattern Recognition Letters* 32 (12) (2011) 1598–1603.
- [46] Y. Pang, Y. Yuan, X. Li, J. Pan, Efficient hog human detection, *Signal Process.* 91 (4) (2011) 773–781.
- [47] B.A. Olshausen, D.J. Field, Sparse coding with an overcomplete basis set: a strategy employed by V1? *Vis. Res.* 37 (23) (1997) 3311–3325.
- [48] S.S. Chen, D.L. Donoho, M.A. Saunders, *Atomic Decomposition by Basis Pursuit*, Society for Industrial and Applied Mathematics, 1998.
- [49] D.L. Donoho, For most large underdetermined systems of linear equations the minimal l_1 -norm solution is also the sparsest solution, *Commun. Pure Appl. Math.* 59 (6) (2006) 797–829.
- [50] R. Tibshirani, Regression shrinkage and selection via the lasso, *J. R. Stat. Soc. 73 (3) (2011) 273–282.*
- [51] H. Yang, Y. Fang, W. Lin, Z. Wang, Subjective quality assessment of screen content images, in: Proceedings of the Sixth International Workshop on Quality of Multimedia Experience, 2014, pp. 257–262.
- [52] Z. Pan, H. Shen, Y. Lu, S. Li, N. Yu, A low-complexity screen compression scheme for interactive screen sharing, *IEEE Trans. Circuits Syst. Video Technol.* 23 (6) (2013) 949–960.
- [53] P.G. Gottschalk, J.R. Dunn, The five-parameter logistic: a characterization and comparison with the four-parameter logistic, *Anal. Biochem.* 343 (1) (2005) 54–65.